

Graphic abstract: Large CP violation in charmed baryon decays arises from the interference between the two contributing diagrams

Large CP violation in charmed baryon decays

Xiao-Gang He^{1,2,*} and Chia-Wei Liu^{1,2,†}

¹*State Key Laboratory of Dark Matter Physics, Tsung-Dao Lee Institute and School of Physics and Astronomy, Shanghai Jiao Tong University, Shanghai 200240, China*

²*Key Laboratory for Particle Astrophysics and Cosmology (MOE) and Shanghai Key Laboratory for Particle Physics and Cosmology, Tsung-Dao Lee Institute and School of Physics and Astronomy, Shanghai Jiao Tong University, Shanghai 200240, China*

(Dated: June 24, 2025)

This work presents the first detailed numerical predictions of CP violation in antitriplet charmed baryon decays. Adopting the flavor $SU(3)_F$ symmetry and the final state re-scattering framework, we relate the CKM-suppressed amplitudes to the leading ones, which are proportional to λ_b and λ_d , respectively, with $\lambda_q = V_{uq}V_{cq}^*$. Larger-than-expected CP violations are found, reaching the order of 10^{-3} , similar in magnitude to those in $D^0 \rightarrow \pi^+\pi^-, K^+K^-$. This opens a promising avenue for observing CP violation in charmed baryon decays and testing the Standard Model.

Received: 13-Mar-2025. Revised: 22-Apr-2025. Accepted: 27-May-2025.

Keywords: CP violation, charm quark, flavor $SU(3)$ symmetry, rare baryon decays.

I. INTRODUCTION

The study of CP violation is fundamentally important as it is closely related to the baryon asymmetry of our universe [1]. Since the CP violation from the Cabibbo-Kobayashi-Maskawa (CKM) matrix $V_{qq'}$ [2] is too small to explain the observed baryon asymmetry, physics beyond the Standard Model (SM) is well motivated. Where the new CP-violating source comes from is still unknown, and the SM should be tested in all possible ways. Systems containing a charm quark host some interesting surprises, such as the CP-violating rate asymmetries of $D^0 \rightarrow \pi^+\pi^-, K^+K^-$ observed at LHCb [3, 4], which are an order of magnitude larger than short-distance (SD) expectations [5]. Although there are speculations taking this as a signal for new physics beyond the SM [6, 7], it has also been argued that if long-distance (LD) contributions are properly taken into account, the SM can accommodate the observed sizes of CP asymmetries [8–10]. To reach a robust conclusion, a lattice QCD simulation is necessary.

We propose to further test CP violation in the charm sector using antitriplet charmed baryon (\mathbf{B}_c) decays into a low-lying octet baryon (\mathbf{B}) and a pseudoscalar meson (P). The decays of charmed mesons and baryons may exhibit similar behavior. The possibility of significant CP violation in \mathbf{B}_c decays should be examined both theoretically and experimentally. Recently, the first evidence of CP violation in baryon decays has been observed in a heavy b -baryon system [11], with magnitudes consistent with SM estimates. It is of great interest to examine whether another heavy baryon sector, the charmed baryon, also exhibits CP violation. Our analysis, based on flavor $SU(3)_F$ symmetry, suggests that testing CP violation in this sector is feasible, potentially with enhanced effects, as seen in $D^0 \rightarrow \pi^+\pi^-, K^+K^-$ decays. This highlights the relevance of two-body charmed baryon decays.

The amplitudes of $\mathbf{B}_c \rightarrow \mathbf{B}P$ are parameterized as $\mathcal{M} = i\bar{u}(F - G\gamma_5)u_c$, where F and G are related to the S wave and P wave, respectively, and $u_{(c)}$ is the Dirac spinor of $\mathbf{B}_{(c)}$. If CP were conserved, F would flip sign and G would remain invariant under the CP transformation. One can construct the CP-violating rate asymmetry $A_{CP} = (\mathcal{B} - \bar{\mathcal{B}})/(\mathcal{B} + \bar{\mathcal{B}})$ and polarization asymmetry $A_{CP}^\alpha = (\alpha + \bar{\alpha})/2$, where $\mathcal{B}(\bar{\mathcal{B}})$ and $\alpha(\bar{\alpha})$ represent the branching fraction and the polarization parameter for the particle (antiparticle), respectively [12].

For non-vanishing A_{CP} and A_{CP}^α , at least two different weak CP-violating phases accompanied by different strong phases are required. Without $K^0 - \bar{K}^0$ mixing it is not possible for Cabibbo-favored (CF) or doubly Cabibbo-suppressed (DCS) processes, but possible for the singly Cabibbo-suppressed (SCS) processes with two weak phases λ_d and $\lambda_s = -\lambda_d - \lambda_b$ with $\lambda_q = V_{cq}^*V_{uq}$. It is significant that the BESIII collaboration observed a sizable phase shift in $\Lambda_c^+ \rightarrow \Xi^0 K^+$ decays [13, 14], suggesting large strong phases within the SM—a key ingredient in the study of CP violation.

Theoretical calculations, starting from the quark-level effective interaction, are challenging due to the strong interactions at the charm scale. No reliable results from first-principles calculations have been established. Methods

* hexg@sjtu.edu.cn

† chiaweiliu@sjtu.edu.cn

based on flavor $SU(3)_F$ symmetry considerations can simplify these calculations in a model-independent manner. It has been demonstrated that $SU(3)_F$ predictions fit data well [15–23]. Nevertheless, this approach cannot provide dynamical details.

We propose a new method for performing the $SU(3)_F$ analysis. At the beginning, we will adopt the usual framework of the $SU(3)_F$ fit. We then reinterpret the fitted parameters in a dynamical model. In particular, we will demonstrate how the fitted amplitudes are related to the dynamical quantities in the framework of the final state re-scattering (FSR). This reinterpretation helps us understand the meanings of the $SU(3)_F$ numerical analysis and give us ways to predict CP violation as will be shown later.

II. MATERIALS AND METHODS

Under the $SU(3)_F$, the effective Lagrangian transforms as $\mathbf{15}$, $\overline{\mathbf{6}}$ and $\mathbf{3}$. The explicit tensor representations responsible for the CF and DCS can be found in Ref. [18]. For the tree-level operators of SCS, we have [24]

$$\mathcal{L}_{eff}^{SCS} = -\frac{G_F}{\sqrt{2}} \sum_{\lambda=\pm} C_\lambda (\mathcal{H}_\lambda)_k^{ij} \bar{q}_i \gamma^\mu (1 - \gamma_5) q^k \bar{q}_j \gamma_\mu (1 - \gamma_5) c, \quad (1)$$

where G_F is the Fermi constant and C_\pm are the Wilson coefficients. The $SU(3)_F$ tensors are defined by

$$(\mathcal{H}_+)_k^{ij} = \frac{\lambda_s - \lambda_d}{2} \mathcal{H}(\mathbf{15}^{s-d})_k^{ij} + \lambda_b \left(\mathcal{H}(\mathbf{15}^b)_k^{ij} + \mathcal{H}(\mathbf{3}_+)^i \delta_k^j + \mathcal{H}(\mathbf{3}_+)^j \delta_k^i \right), \quad (2)$$

and

$$(\mathcal{H}_-)_k^{ij} = \frac{\lambda_s - \lambda_d}{2} \mathcal{H}(\overline{\mathbf{6}})_{kl} \epsilon^{lij} + 2\lambda_b \left(\mathcal{H}(\mathbf{3}_-)^i \delta_k^j - \mathcal{H}(\mathbf{3}_-)^j \delta_k^i \right). \quad (3)$$

By construction \mathcal{H}_+ and \mathcal{H}_- are symmetric and antisymmetric in the two upper indices. The nonzero matrix elements are given as $\mathcal{H}(\overline{\mathbf{6}})_{23} = \mathcal{H}(\mathbf{15}^{s-d})_2^{12} = -\mathcal{H}(\mathbf{15}^{s-d})_3^{13} = -1$, $-2\mathcal{H}(\mathbf{15}^b)_1^{11} = 4\mathcal{H}(\mathbf{15}^b)_2^{12} = 4\mathcal{H}(\mathbf{15}^b)_3^{13} = 4\mathcal{H}(\mathbf{3}_-) = 4\mathcal{H}(\mathbf{3}_+) = -1$ and the others are obtained by $\mathcal{H}(\overline{\mathbf{6}})_{ij} = \mathcal{H}(\overline{\mathbf{6}})_{ji}$ and $\mathcal{H}(\mathbf{15})_k^{ij} = \mathcal{H}(\mathbf{15})_k^{ji}$. Both the $\mathbf{15}$ and $\mathbf{3}$ representations contain components proportional to λ_b . The SD penguin operators transform under $SU(3)_F$ as $\mathbf{3}$. Their Wilson coefficients, $C_{3\sim 6}$, are smaller than $C_{1,2}$ by an order [25]. We will first focus on the effects from the $\mathbf{3}$ in the tree-level operators and then comment on those from the SD penguins at the end.

The interaction operators have been grouped according to $SU(3)_F$, and the same grouping can be applied to the initial and final hadron states. The antitriplet $(\mathbf{B}_c)_i$ contains $(\Xi_c^0, \Xi_c^+, \Lambda_c^+)_i$, while \mathbf{B} and P belong to the $\mathbf{8}$ representations, labelled as \mathbf{B}_j^i and P_j^i including $\{p, n, \Lambda, \Sigma^{\pm,0}, \Xi^{0,-}\}$ and $\{\pi^{\pm,0}, \eta_8, K^{\pm,0}, \overline{K}^0\}$ as elements, respectively [21]. Note that η_8 is a mixture of the physical η and η' , which will not be discussed here.

The effective Lagrangian at the hadron level is obtained by writing all possible $SU(3)_F$ contractions among $(\mathbf{B}_c)_i$, $(\mathbf{B})_j^i$, $(P^\dagger)_j^i$ and $(\mathcal{H}_\pm)_k^{ij}$. For each contraction, we assign an unknown parameter \tilde{f} and \tilde{g} for the S and P waves, respectively. The effective Lagrangian for S wave at the hadron level is then given by [21]

$$\begin{aligned} \mathcal{L}_{\mathbf{B}_c \mathbf{B} P} &= (P^\dagger)_n^l \overline{\mathbf{B}}_m^k \left(\frac{\lambda_s - \lambda_d}{2} (F^{s-d})_{ijkl}^{mn} \epsilon^{ijn} (\mathbf{B}_c)_n + \lambda_b (F^b)_{kl}^{imn} (\mathbf{B}_c)_i \right) + (\text{H.c.}), \\ (F^{s-d})_{ijkl}^{mn} &= \tilde{f}^b \mathcal{H}(\overline{\mathbf{6}})_{il} \delta_k^n \delta_j^m + \tilde{f}^c \mathcal{H}(\overline{\mathbf{6}})_{ik} \delta_j^n (\delta^\dagger)_l^m + \tilde{f}^d \mathcal{H}(\overline{\mathbf{6}})_{kl} \delta_j^n (\delta^\dagger)_i^m + \tilde{f}^e \mathcal{H}(\mathbf{15}^{s-d})_l^{mn} \epsilon_{ijk} / 2, \\ (F^b)_{kl}^{imn} &= \tilde{f}^e \mathcal{H}(\mathbf{15}^b)_l^{mn} \delta_k^i + \tilde{f}_3^b \delta_l^i \mathcal{H}(\mathbf{3})^m \delta_k^n + \tilde{f}_3^c \mathcal{H}(\mathbf{3})^i \delta_l^m \delta_k^n + \tilde{f}_3^d \mathcal{H}(\mathbf{3})^n \delta_l^m \delta_k^i, \end{aligned} \quad (4)$$

where we have recombined $\mathcal{H}(\mathbf{3}_+)$ and $\mathcal{H}(\mathbf{3}_-)$ into $\mathcal{H}(\mathbf{3}) = (1, 0, 0)$, and \tilde{f} are the $SU(3)_F$ amplitudes. Since the S and P waves share the same flavor structure, Eq. (4) holds after the substitution of $(F, \tilde{f}) \rightarrow (-G, \tilde{g})$ [21]. The Körner-Patti-Woo (KPW) theorem [26–28] had been applied to eliminate several redundant terms associated with $\mathcal{H}(\mathbf{15})$. We will use \tilde{h} as a generic label for either \tilde{f} or \tilde{g} , and \tilde{h}_3 denotes any of $\tilde{h}_3^{b,c,d}$

Interestingly, \tilde{f}^e appears in both F^{s-d} and F^b . Even if \tilde{h}_3 are dropped, one can still have nonzero A_{CP} and A_{CP}^α from \tilde{h}^e , which can be determined from CP-even data. In this case A_{CP} and A_{CP}^α are proportional to $\lambda_b \tilde{h}^e$. Numerical results on CP-violating quantities in this scenario are of the order of $\mathcal{O}(10^{-4})$ as will be shown in the next section. The sizes of A_{CP} are significantly smaller than the ones of D meson [3]. One wonders if enhanced CP-violating effects can appear as those showed up in $D \rightarrow \pi^+ \pi^-, K^+ K^-$. If this indeed happens, it must come from \tilde{h}_3 .

To estimate the sizes of \tilde{h}_3 , we adopt a model analysis combining the SD tree-emissions and FSR effects. Within this framework, the full effective Lagrangian for $\mathbf{B}_c \rightarrow \mathbf{B} P$ at the hadron level is decomposed into three parts:

$$\mathcal{L}_{\mathbf{B}_c \mathbf{B} P} = \mathcal{L}_{\mathbf{B}_c \mathbf{B} P}^{\text{Tree}} + \mathcal{L}_{\mathbf{B}_c \mathbf{B} P}^{\text{FSR-s}} + \mathcal{L}_{\mathbf{B}_c \mathbf{B} P}^{\text{FSR-t}}. \quad (5)$$

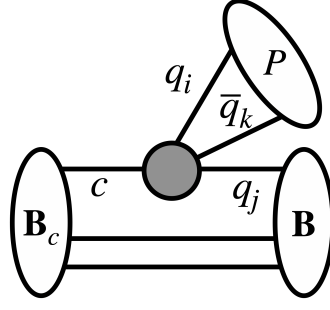


Fig. 1. Topological diagram for $\mathcal{L}_{\mathbf{B}_c \mathbf{B} P}^{\text{Tree}}$, where the middle blob indicates the insertion of $\mathcal{L}_{eff}^{\text{SCS}}$.

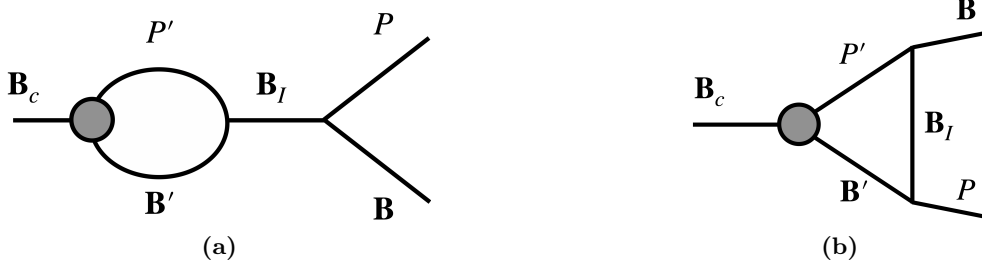


Fig. 2. The left(right) diagram represents the $s(t)$ -channel FSR with the blob representing the SD weak transition induced by $\mathcal{L}_{\mathbf{B}_c \mathbf{B} P}^{\text{Tree}}$. Here we consider elastic re-scattering such that \mathbf{B}' and P' belong to the same $SU(3)_F$ octets as \mathbf{B} and P , respectively.

$$\begin{aligned}
 & \mathcal{L}_{\mathbf{B}_c \mathbf{B} P}^{\text{FSR-s}} = \sum_{\mathbf{B}', P', \mathbf{B}_I} \left(\begin{array}{c} \text{Diagram with blob } \mathcal{H}_{-}^{ij} \text{ and vertices } (\mathbf{B}_c)_l, (\mathbf{B}_I)_{k_2}, (\overline{\mathbf{B}}_I)_{i_1}, (\mathbf{B}')_{j_2}, (\overline{\mathbf{B}})_{k_2}, (\mathbf{B}')_{j_1}, (\mathbf{B})_{k_1} \\ + r_- \left(\begin{smallmatrix} i_1 & \leftrightarrow & j_1 \\ j_1 & & k_1 \end{smallmatrix} \right) + r_- \left(\begin{smallmatrix} i_2 & \leftrightarrow & j_2 \\ j_2 & & k_2 \end{smallmatrix} \right) + r_-^2 \left(\begin{smallmatrix} i_1 & \leftrightarrow & j_1, & i_2 & \leftrightarrow & j_2 \\ j_1 & & k_1, & j_2 & & k_2 \end{smallmatrix} \right) \end{array} \right)
 \end{aligned}$$

Fig. 3. A pictorial explanation of Eq. (8). The square blob on the left-hand side represents the insertion of $\mathcal{L}_{\mathbf{B}_c \mathbf{B} P}^{\text{FSR-s}}$, while the circle blob on the right stands for $\mathcal{L}_{\mathbf{B}_c \mathbf{B}' P'}^{\text{Tree}}$. The other vertices are strong couplings.

The first term is induced by the SD tree emission depicted in Fig. 1, while the second (third) term is responsible for the LD $s(t)$ -channel elastic re-scattering depicted in Fig. 2, where \mathbf{B}' and P' also belong to the same $SU(3)_F$ octets as \mathbf{B} and P . Studies have shown that multi-meson re-scattering is suppressed compared to two-to-two particle re-scattering at the charm energy scale [29]. We will also work with this approximation for the baryon-meson re-scattering.

The main goal is to determine the $SU(3)_F$ structure of the FSR; in other words, the relationship between F^{s-d} and F^b in Eq. (4). Since the former has already been determined in the global $SU(3)_F$ fit from CP-even data, we can immediately determine the latter once their relationship has been established.

According to Fig. 1, the tree-emission diagram has the flavor structure of

$$\mathcal{L}_{\mathbf{B}_c \mathbf{B} P}^{\text{Tree}} = (P^\dagger)_i^k (\overline{\mathbf{B}})_j^l \left(\tilde{F}_V^+ (\mathcal{H}_+)^{ij} + \tilde{F}_V^- (\mathcal{H}_-)^{ij} \right) (\mathbf{B}_c)_l. \quad (6)$$

The parameters \tilde{F}_V^+ and \tilde{F}_V^- represent the overall unknowns. By replacing \tilde{F}_V^\pm with \tilde{G}_A^\pm and inserting γ_5 , we obtain the result for the P wave. We follow the the generalized factorization approach [30, 31], which introduces effective color numbers in the S- and P-wave amplitudes as unknown parameters. In the most general case, the effective color

numbers can be complex, and the S- and P-wave amplitudes may have different values. To account for this, we factor out these unknowns and absorb them into the definitions of \tilde{F}_V^\pm and \tilde{G}_A^\pm , which are treated as free parameters in our analysis.

By decomposing \mathcal{H}_\pm according to Eqs. (2) and (3), we see **15**, $\bar{\mathbf{6}}$, and **3** share two parameters, \tilde{F}_V^+ and \tilde{F}_V^- in $\mathcal{L}_{\mathbf{B}_c\mathbf{B}P}^{\text{Tree}}$. Hence, once the amplitudes for **15** and $\bar{\mathbf{6}}$ are determined, the amplitude for **3** is fixed. The ability to achieve this in $\mathcal{L}_{\mathbf{B}_c\mathbf{B}P}^{\text{Tree}}$ stems from the fact that \mathcal{H}_+ fixes the ratio of contributions between **15** and **3**₊, while \mathcal{H}_- fixes the ratio between $\bar{\mathbf{6}}$ and **3**₋. Later, we will show that the same can be done in the *s*- and *t*-channel FSR.

For illustration, we carry out the $SU(3)_F$ analysis of the *s*-channel. The *s*(*t*)-channel FSR diagram is given in Fig. 2a(2b) where the blob represents the SD weak transition induced by $\mathcal{L}_{\mathbf{B}_c\mathbf{B}P}^{\text{Tree}}$. The other vertices are strong couplings among the hadrons induced by $\mathcal{L}_{\mathbf{B}_\pm\mathbf{B}P}^{\text{strong}}$:

$$\mathcal{L}_{\mathbf{B}_-\mathbf{B}P}^{\text{strong}} = g_- \left((P^\dagger)_j^i (\bar{\mathbf{B}}')_k^j + r_- (P^\dagger)_k^j (\bar{\mathbf{B}}')_j^i \right) (\mathbf{B}_-)_i^k + (\text{H.c.}), \quad (7)$$

where the subscript of \pm denotes the parity of \mathbf{B}_\pm , and g_\pm and r_\pm are constants. The $SU(3)_F$ structure of $\mathcal{L}_{\mathbf{B}_+\mathbf{B}P}^{\text{strong}}$ is the same as that of $\mathcal{L}_{\mathbf{B}_-\mathbf{B}P}^{\text{strong}}$ and is obtained by replacing (g_-, r_-) with (g_+, r_+) and inserting $i\gamma_5$ between the baryons in Eq. (7). The intermediate baryons \mathbf{B}_I can have either parity. In addition to the case where \mathbf{B}_I belongs to the same $SU(3)_F$ octet as \mathbf{B} , we also consider the scenario where \mathbf{B}_I is one of the low-lying negative-parity octet baryons, such as $N(1535)$, $\Sigma(1620)$, and $\Lambda(1670)$, as they are expected to have the largest couplings.

To determine r_+ , we use input from the Taylor series extrapolation [32], which yields $r_+ \approx 2.47$. For r_- , we perform a χ^2 fit on the experimental two-body decay widths of $N(1535) \rightarrow N\pi, N\eta, \Sigma(1620) \rightarrow N\bar{K}, \Lambda\pi, \Sigma\pi$, and $\Lambda(1670) \rightarrow N\bar{K}, \Sigma\pi, \Lambda\eta$ [33]. The best-fit solution yields $r_- = 2.45 \pm 0.81$. The values of g_\pm can also be extracted using the same procedure as r_\pm . However, their numerical values do not impact the results in our analysis, as they can be absorbed into the overall unknowns. To account for the running of r_\pm with respect to the energy scale, we adopt a wide range of values for $r_+ = r_- = 2.5 \pm 0.8$ for illustration.

Now, we derive the $SU(3)_F$ structure of the *s*-channel FSR. We use the S wave as an illustration. By viewing Fig. 2a, we see that $\mathcal{L}_{\mathbf{B}_c\mathbf{B}P}^{\text{FSR-s}}$ consists of one $\mathcal{L}_{\mathbf{B}_c\mathbf{B}P}^{\text{Tree}}$ and two $\mathcal{L}_{\mathbf{B}_-\mathbf{B}P}^{\text{strong}}$. Contracting the hadron operators according to the topology of Fig. 2a, we arrive at

$$\begin{aligned} -\langle \mathcal{L}_{\mathbf{B}_c\mathbf{B}P}^{\text{FSR-s}} \rangle &= \sum_{\mathbf{B}_I, \mathbf{B}', P'} \left\langle \mathcal{L}_{\mathbf{B}_I\mathbf{B}P}^{\text{strong}} \mathcal{L}_{\mathbf{B}_I\mathbf{B}'P'}^{\text{strong}} \mathcal{L}_{\mathbf{B}_c\mathbf{B}'P'}^{\text{Tree}} \right\rangle_{\text{FSR-s}} \\ &= \frac{1}{8} \sum_{a,b,c=1}^8 \left\langle g_-^2 \tilde{F}_V^- \left((P^\dagger)_{j_1}^{i_1} (\bar{\mathbf{B}})_{k_1}^{j_1} (\mathbf{B}_I^-)_a (\lambda_a)_{i_1}^{k_1} \right) \left(P'_c (\lambda_c)_{j_2}^{i_2} (\bar{\mathbf{B}}_I^-)_a (\lambda_a)_{k_2}^{j_2} \mathbf{B}'_b (\lambda_b)_{i_2}^{k_2} \right) \left(P'^\dagger (\lambda_c)_i^k \bar{\mathbf{B}}'_b (\lambda_b)_j^l (\mathcal{H}_-)^{ij}_k (\mathbf{B}_c)_l \right) \right\rangle \\ &\quad + r_- \left(\begin{smallmatrix} i_1 & \leftrightarrow & j_1 \\ j_1 & & k_1 \end{smallmatrix} \right) + r_- \left(\begin{smallmatrix} i_2 & \leftrightarrow & j_2 \\ j_2 & & k_2 \end{smallmatrix} \right) + r_-^2 \left(\begin{smallmatrix} i_1 & \leftrightarrow & j_1, & i_2 & \leftrightarrow & j_2 \\ j_1 & & k_1, & j_2 & & k_2 \end{smallmatrix} \right). \end{aligned} \quad (8)$$

Fig. 3 provides a pictorial description of the above equation, omitting the overall couplings. In the second line, we use Eq. (7) to expand $\mathcal{L}_{\mathbf{B}_-\mathbf{B}P}^{\text{strong}}$ and decompose the hadrons as $(h)_j^i = \frac{1}{\sqrt{2}} \sum_{a=1}^8 h_a (\lambda_a)_j^i$, where $(\lambda_a)_j^i$ are the Gell-Mann matrices and $h = \mathbf{B}', \mathbf{B}_I^-, P'$. This decomposition arises because these hadrons belong to the **8** representation. In the second equation, $\left(\begin{smallmatrix} i_1 & \leftrightarrow & j_1 \\ j_1 & & k_1 \end{smallmatrix} \right)$ denotes the term obtained by swapping i_1 and j_1 in the upper indices and j_1 and k_1 in the lower indices of the first term. The contributions of \mathcal{H}_+ in $\mathcal{L}_{\mathbf{B}_c\mathbf{B}P}^{\text{FSR-s}(t)}$ vanish due to the KPW theorem.

In the momentum basis, the Wick contractions in Eq. (8) are collectively replaced by the hadron propagators with a loop integral:

$$\tilde{S}^- \equiv \int \frac{d^4q}{48\pi^4} \frac{g_-^2 \tilde{F}_V^-}{(q - p_{\mathbf{B}_c})^2 - m_{P'}^2} \frac{p_{\mathbf{B}_c}^\mu \gamma_\mu + m_{\mathbf{B}_I} q^\mu \gamma_\mu + m_{\mathbf{B}'}}{p_{\mathbf{B}_c}^2 - m_{\mathbf{B}_I}^2} \frac{q^\mu \gamma_\mu + m_{\mathbf{B}'}}{q^2 - m_{\mathbf{B}'}^2}. \quad (9)$$

Clearly, the above integral is independent of the indices (a, b, c) since the masses $m_{\mathbf{B}_I, \mathbf{B}', P'}$ remain unchanged in the $SU(3)_F$ limit. Substituting the overall factor \tilde{S}^- defined above, Eq. (8) can be rewritten as:

$$\begin{aligned} \mathcal{L}_{\mathbf{B}_c\mathbf{B}P}^{\text{FSR-s}} &= \frac{3\tilde{S}^-}{8} \sum_{a,b,c=1}^8 (P^\dagger)_{j_1}^{i_1} (\bar{\mathbf{B}})_{k_1}^{j_1} (\lambda_a)_{i_1}^{k_1} (\lambda_c)_{j_2}^{i_2} (\lambda_a)_{k_2}^{j_2} (\lambda_b)_{i_2}^{k_2} (\lambda_c)_i^k (\lambda_b)_j^l (\mathcal{H}_-)^{ij}_k (\mathbf{B}_c)_l \\ &\quad + r_- \left(\begin{smallmatrix} i_1 & \leftrightarrow & j_1 \\ j_1 & & k_1 \end{smallmatrix} \right) + r_- \left(\begin{smallmatrix} i_2 & \leftrightarrow & j_2 \\ j_2 & & k_2 \end{smallmatrix} \right) + r_-^2 \left(\begin{smallmatrix} i_1 & \leftrightarrow & j_1, & i_2 & \leftrightarrow & j_2 \\ j_1 & & k_1, & j_2 & & k_2 \end{smallmatrix} \right). \end{aligned} \quad (10)$$

Note that \tilde{S}^- contains unknown information regarding the momentum dependencies of \tilde{F}_V^- and g_\pm in loop integrals, so it is treated as an independent parameter. We can get rid of Gell-Mann matrices by the completeness relation of $\sum_a (\lambda_a)_j^i (\lambda_a)_l^k = 2(\delta_l^i \delta_j^k - \delta_j^i \delta_l^k/3)$. Carrying out the same reduction rules for $\mathcal{L}_{\mathbf{B}, \mathbf{B}P}^{\text{FSR-}t}$, we match Eq. (5) to (4) and find

$$\begin{aligned}\tilde{f}^b &= \tilde{F}_V^- - (r_- + 4)\tilde{S}^- + \sum_{\lambda=\pm} (2r_\lambda^2 - r_\lambda)\tilde{T}_\lambda^-, \\ \tilde{f}^c &= -r_-(r_- + 4)\tilde{S}^- + \sum_{\lambda=\pm} (r_\lambda^2 - 2r_\lambda + 3)\tilde{T}_\lambda^-, \\ \tilde{f}^d &= \tilde{F}_V^- + \sum_{\lambda=\pm} (2r_\lambda^2 - 2r_\lambda - 4)\tilde{T}_\lambda^-, \quad \tilde{f}^e = \tilde{F}_V^+, \end{aligned}\tag{11}$$

for the CKM-leading amplitudes. Here \tilde{T}_\pm^- represent the overall unknown constants in the t -channel S-wave FSR with the subscript denoting the \mathbf{B}_I parity. For the CKM-suppressed amplitudes, we have that

$$\begin{aligned}\tilde{f}_3^b &= (1 - \frac{7r_-}{2})\tilde{S}^- + \sum_{\lambda=\pm} (r_\lambda^2 - 5r_\lambda/2 + 1)\tilde{T}_\lambda^-, \\ \tilde{f}_3^c &= \frac{(r_- + 1)(7r_- - 2)}{6}\tilde{S}^- - \sum_{\lambda=\pm} \frac{r_\lambda^2 + 11r_\lambda + 1}{6}\tilde{T}_\lambda^-, \\ \tilde{f}_3^d &= \frac{2r_- - 7r_-^2}{2}\tilde{S}^- + \sum_{\lambda=\pm} \frac{(r_\lambda + 1)^2}{2}\tilde{T}_\lambda^- - \frac{\tilde{F}_V^+ + 2\tilde{F}_V^-}{4}. \end{aligned}\tag{12}$$

The P-wave relations can be obtained by replacing $(\tilde{f}, \tilde{F}_V^\pm, \tilde{S}^-, \tilde{T}_\pm^-, r_\pm)$ by $(-\tilde{g}, \tilde{G}_A^\pm, \tilde{S}^+, \tilde{T}_\mp^+, r_\mp)$ with $\tilde{S}^+(\tilde{T}_\pm^+)$ an overall unknown in P-wave $s(t)$ -channel. Earlier, we have determined $r_- = r_+ = 2.5 \pm 0.8$. We combine the summations of λ in Eqs. (11) and (12) and redefine $\tilde{T}^\pm = (\tilde{T}_+^\pm + \tilde{T}_-^\pm)$.

III. RESULTS

With the formula given in the previous section, we determine $\tilde{h}^{b,c,d,e}$ from CP-conserving data first, then use Eqs. (11) and (12) to determine $\tilde{h}_3^{b,c,d}$, and finally obtain CP violation predictions.

In Table I, we present the extracted values of $\tilde{h}^{b,c,d,e}$ obtained using the minimal χ^2 fitting method described in Ref. [21], incorporating the latest experimental data [12, 34–39]. We stress that all experimental data available as of March 2025 have been included in our analysis. Given that the current data focus on CP-even quantities and $\lambda_d \gg \lambda_b$, we omitted \tilde{h}_3 in the $SU(3)_F$ fit, but it will be included when discussing CP violation later. The deviation between the current and previous fitted $\tilde{h}^{b,c,d,e}$ arises primarily from the double Z_2 ambiguities inherent in the $SU(3)_F$ framework [21] when precise measurements of the Lee–Yang parameters were unavailable. In our earlier analysis, the lack of reliable input for γ forced us to choose a solution corresponding to a negative value of $\gamma(\Lambda_c^+ \rightarrow \Lambda\pi^+)$ [40], which has since been ruled out by the recent high-precision measurement from LHCb [36]. As a result, the newly adopted solution, consistent with the experimentally determined positive γ , leads to a different set of \tilde{h} . Nevertheless, the predicted \mathcal{B} and α are similar to our previous work as they are invariant under the Z_2 transformations. Hence, A_{CP} and A_{CP}^α calculated from the two sets of parameters will have similar values.

The result χ^2 per degree of freedom is 2.9, indicating a certain level of discrepancy. It is worth pointing out that a recent lattice simulation found $\mathcal{B}(\Xi_c^0 \rightarrow \Xi^- e^+ \nu_e) = (3.58 \pm 0.12)\%$ [41], which is about three times larger than the experimental value $(1.05 \pm 0.20)\%$ [33]. Nevertheless, the lattice result is in good agreement with the $SU(3)_F$ -based prediction $\mathcal{B}(\Xi_c^0 \rightarrow \Xi^- e^+ \nu_e) = (4.10 \pm 0.46)\%$ [42]. A likely explanation for the discrepancy is that the normalization channel of Ξ_c^0 was underestimated in experiments [21], which in turn led to underestimations of all decay branching fractions of Ξ_c^0 [41]. Remarkably, the reconstructed prediction $\mathcal{B}(\Xi_c^0 \rightarrow \Xi^- K^+) = (1.26 \pm 0.04) \times 10^{-3}$ is also about three times larger than the experimental value $(3.9 \pm 1.1) \times 10^{-4}$ [33], mirroring the same factor of discrepancy seen in the semileptonic decay. Upcoming experimental measurements may clarify the source of this discrepancy. In this work, however, we focus on CP violation and therefore adhere to exact $SU(3)_F$ symmetry and the original data. A comprehensive analysis of the fitting issues with other theoretical considerations, such as $SU(3)_F$ breaking, will be presented elsewhere.

In the framework of FSR, the unknown parameters $(\tilde{F}_V^\pm, \tilde{S}^-, \tilde{T}^-)$ and $(\tilde{G}_A^\pm, \tilde{S}^+, \tilde{T}^+)$ can be determined using Eq. (11) and the inputs $\tilde{h}^{b,c,d,e}$ obtained from the global fit. Subsequently, we obtain \tilde{h}_3 from Eq. (12). We observe

	\tilde{h}^b	\tilde{h}^c	\tilde{h}^d	\tilde{h}^e	\tilde{h}_3^b	\tilde{h}_3^c	\tilde{h}_3^d
$ \tilde{f} $	6.75(67)	2.88(15)	1.68(60)	1.17(58)	0.70(11)(1)	4.37(21) (97)	5.12(49) (2.61)
δ_f	0	0.35(6)	-0.05(12)	-2.80(27)	0.90(10)(62)	-3.07(4)(3)	0.22(7)(15)
$ \tilde{g} $	23.47(1.11)	9.62(44)	6.14(1.91)	0.40(0.63)	9.09(18)(4.67)	10.46(62)(19)	1.99(2.25)(4.72)
δ_g	2.49(11)	-1.17(9)	2.89(31)	-0.97(6.10)	-1.01(6)(3)	-0.69(12)(6)	-2.07(75)(1.09)

Table I. The $SU(3)_F$ parameters are given by $\tilde{h} = |\tilde{h}| \exp(i\delta_h)$. The values of $\tilde{h}^{b,c,d,e}$ are determined from a global $SU(3)_F$ fit, while those of \tilde{h}_3 are obtained in the framework of FSR. In the global fit for Λ_c^+ , we use the absolute experimental branching fractions, as the normalization channel $\Lambda_c^+ \rightarrow pK^-\pi^+$ is well measured with minimal uncertainties [33]. For Ξ_c decay data we use the absolute branching fraction for $\Xi_c^0 \rightarrow \Xi^-\pi^+$ while employing relative ratios for the other Ξ_c^0 decays with $\Xi_c^0 \rightarrow \Xi^-\pi^+$ the normalized channel. On the other hand, we use absolute branching fractions for Ξ_c^+ with $\Xi_c^+ \rightarrow \Xi^-\pi^+\pi^+$ the normalized channel [33, 39], as the three-body decays are not parameterized in our framework of the $SU(3)_F$ symmetry. The magnitudes $|\tilde{h}|$ and phases δ_h are expressed in units of $10^{-2}G_F \text{ GeV}^2$ and radians, respectively. Values within parentheses represent the last two digits of the uncertainties, such as $6.75(67) = 6.75 \pm 0.67$. The first uncertainties arise from the experimental input, while the second uncertainties arise from the hadron couplings.

Channels	\mathcal{B}	A_{CP}	A_{CP}^α	Channels	\mathcal{B}	A_{CP}	A_{CP}^α
$\Lambda_c^+ \rightarrow p\pi^0$	0.18(2)	-0.01(7)	-0.15(13)	$\Xi_c^0 \rightarrow \Sigma^+\pi^-$	0.26(2)	0	0
		0.01(15)(45)	0.55(20)(61)			0.71(15)(6)	-1.83(10)(15)
$\Lambda_c^+ \rightarrow n\pi^+$	0.68(6)	0.0(1)	0.03(2)	$\Xi_c^0 \rightarrow \Sigma^0\pi^0$	0.34(3)	-0.02(4)	0.01(1)
		-0.02(7)(28)	0.30(13)(41)			0.44(24)(17)	-0.43(31)(16)
$\Lambda_c^+ \rightarrow \Lambda K^+$	0.62(3)	0.00(2)	0.03(2)	$\Xi_c^0 \rightarrow \Sigma^-\pi^+$	1.76(5)	0.01(1)	-0.01(1)
		-0.15(13)(9)	0.50(9)(21)			0.12(6)(2)	-0.22(5)(21)
$\Xi_c^+ \rightarrow \Sigma^+\pi^0$	2.69(14)	-0.02(6)	0.07(4)	$\Xi_c^0 \rightarrow \Xi^0 K_{S/L}$	0.38(1)	0	0
		0.05(7)(8)	-0.23(3)(15)			0.18(3)(5)	-0.38(2)(11)
$\Xi_c^+ \rightarrow \Sigma^0\pi^+$	3.14(10)	0.00(1)	-0.02(1)	$\Xi_c^0 \rightarrow \Xi^- K^+$	1.26(4)	0.00(1)	0.01(1)
		0.05(8)(7)	-0.24(6)(13)			-0.12(5)(2)	0.21(4)(2)
$\Xi_c^+ \rightarrow \Xi^0 K^+$	1.30(10)	0.00(0)	-0.02(1)	$\Xi_c^0 \rightarrow pK^-$	0.31(2)	0	0
		0.01(6)(17)	-0.23(9)(52)			-0.73(18)(6)	1.74(11)(14)
$\Xi_c^+ \rightarrow \Lambda\pi^+$	0.18(3)	-0.01(2)	0.0(0)	$\Xi_c^0 \rightarrow nK_{S/L}$	0.86(3)	0	0
		-0.31(21)(13)	0.96(25)(44)			-0.14(3)(4)	0.27(2)(7)
$\Xi_c^+ \rightarrow pK_s$	1.55(7)	0	0	$\Xi_c^0 \rightarrow \Lambda\pi^0$	0.06(2)	0.02(3)	0.0(1)
		-0.13(3)(4)	0.22(3)(7)			-0.12(18)(10)	0.69(8)(43)

Table II. The \mathcal{B} , A_{CP} , and A_{CP}^α are presented in units of 10^{-3} . The upper rows of A_{CP} and A_{CP}^α are obtained by taking $\tilde{h}_3 = 0$, while the lower rows are obtained through the FSR mechanism. The uncertainties are quoted in the same manner as Table I. There may be some $SU(3)_F$ breaking effects that affect the results on the order of 10^{-1} , as found in the hyperons.

that their absolute values are of the same order as those of $\tilde{h}^{b,c,d,e}$, which may lead to sizable CP violation. The predicted values of A_{CP} and A_{CP}^α , based on the omission of \tilde{h}_3 , are shown in the upper rows of Table II. On the other hand, the values of A_{CP} and A_{CP}^α obtained by solving for \tilde{h}_3 within the framework of FSR are listed in the lower row of the same table. The values of A_{CP} are typically enhanced to the order of 10^{-3} , consistent with the observed enhancement of CP violation in D meson decays.

IV. DISCUSSION AND CONCLUSION

Under the U-spin symmetry, an $SU(2)$ subgroup of $SU(3)_F$ between d and s , exchanging d and s in the initial and final states can be viewed as taking the transformation of $(\lambda_s - \lambda_d, \lambda_b) \rightarrow (-\lambda_s + \lambda_d, \lambda_b)$. Since CP asymmetries are proportional to $\text{Im}(\lambda_b^*(\lambda_s - \lambda_d))$, they flip signs after exchanging d and s in the initial and final states. This kind of

$SU(3)_F$ relation provides useful information to test the CKM mechanism model-independently [43]. From the U-spin symmetry we have [15, 44]

$$\begin{aligned} A_{CP}(\Xi_c^0 \rightarrow \Xi^0 K_{S/L}^0) &= -A_{CP}(\Xi_c^0 \rightarrow n K_{S/L}^0), \\ A_{CP}(\Xi_c^0 \rightarrow \Sigma^- \pi^+) &= -A_{CP}(\Xi_c^0 \rightarrow \Xi^- K^+), \\ A_{CP}(\Xi_c^0 \rightarrow \Sigma^+ \pi^-) &= -A_{CP}(\Xi_c^0 \rightarrow p K^-). \end{aligned} \quad (13)$$

These direct relations also apply when substituting A_{CP}^α for A_{CP} .

The above U-spin relations may help reduce systematic errors in experiments, in the same spirit as $A_{CP}(D^0 \rightarrow \pi^+ \pi^-) - A_{CP}(D^0 \rightarrow K^+ K^-)$. Specifically, we recommend measuring $A_{CP}(\Xi_c^0 \rightarrow p K^-) - A_{CP}(\Xi_c^0 \rightarrow \Sigma^+ \pi^-)$ and $A_{CP}^\alpha(\Xi_c^0 \rightarrow p K^-) - A_{CP}^\alpha(\Xi_c^0 \rightarrow \Sigma^+ \pi^-)$, which, according to our analysis, are found to be $(-1.44 \pm 0.35) \times 10^{-3}$ and $(3.57 \pm 0.36) \times 10^{-3}$, respectively. All the final states are charged, making them ideal channels to probe CP violation in baryon decays. The intuitive reason why these two channels exhibit large CP violation can be traced to two similar topological diagrams, as shown in the graphic abstract. The diagrams are comparable in magnitude, allowing for significant interference between $V_{cd}^* V_{ud}$ and $V_{cs}^* V_{us}$.

Data from LHCb revealed significant U-spin breaking in D^0 decays [4]. Resonances $f(1710)$ and $f(1790)$, which are close in mass to D mesons, are thought to contribute significantly to $SU(3)_F$ breaking in D^0 decays [45, 46]. Conversely, no similar mechanism is expected in charmed baryons, and good $SU(3)_F$ fits indicate that $SU(3)_F$ is applicable to the precision we are interested in [21, 41, 42]. Large deviations of U-spin symmetry are not expected, providing valuable experimental tests for the SM. To be conservative, one should note that $SU(3)_F$ breaking may affect our predictions on the order of 10^{-1} as found in the hyperons. Nevertheless, the breaking should not affect the overall sizes of CP asymmetries, found to be 10^{-3} in this work.

Before ending the discussion, we would like to comment on the SD penguin operators which have been neglected so far. We estimate their sizes with the naive factorization. In this framework, the SD penguin operators will scale the last term $-(\tilde{F}_V^+ + 2\tilde{F}_V^-)/4$ in \tilde{f}_3^d in Eq. (12) by a factor of $(1 + \mathcal{R}_+)$ with $\mathcal{R}_\pm = (3C_4 + C_3)/C_1 \pm m_K^2(6C_6 + 2C_5)/(m_s m_c C_1)$ and similarly $-(\tilde{G}_A^+ + 2\tilde{G}_A^-)/4$ in \tilde{g}_3^d by a factor of $(1 + \mathcal{R}_-)$. We have checked that the corrections on A_{CP} and A_{CP}^α are less than 10%, which can be neglected.

It should also be noted that although our framework is built upon the SM, our $SU(3)_F$ fit may partially absorb new physics contributions. From the results we have obtained, we would like to conclude that there is no clear evidence indicating the need for physics beyond the SM to explain the data. A significant number of charmed baryons will be produced in the near future. Thus far, Belle's dataset has achieved measurements of A_{CP} and A_{CP}^α with precision at the percent level [47]. Belle II is expected to increase production, achieving precision at the subpercent level. At LHCb, the production rates of charmed baryons are suppressed to around 30% compared to D mesons [48], but the precision of A_{CP} may also reach 10^{-3} . Following the High Luminosity upgrade [49], the integrated luminosity is expected to increase tenfold. In the future, the Super τ -Charm Facility may also provide valuable data on these decays [50, 51]. The enhancement identified in this work facilitates the first observation of CP violation in two-body charmed baryon decays.

CONFLICT OF INTEREST

The authors declare that they have no conflict of interest.

ACKNOWLEDGMENTS

This work is supported in part by the National Key Research and Development Program of China 2020YFC2201501, the National Natural Science Foundation of China (12090064, 12205063, 12375088, and W2441004), and the China Postdoctoral Science Foundation 2023M742293.

AUTHOR CONTRIBUTIONS

The project originated from a mutual discussion on possible large CP violation in charmed baryon decays. Xiao-Gang He formulated the overall strategy, and Chia-Wei Liu developed key methods to pursue the analysis. Both

authors contributed equally to the research and manuscript preparation.

-
- [1] Sakharov AD, Violation of CP invariance, C asymmetry, and baryon asymmetry of the universe, *JETP Lett* **5**, 32-35 (1967).
- [2] Kobayashi M, Maskawa T, CP violation in the renormalizable theory of weak interaction, *Prog Theor Phys* **49**, 652-657 (1973).
- [3] LHCb Collaboration, R Aaij et al., Observation of CP violation in charm decays, *Phys Rev Lett* **122**, 211803 (2019).
- [4] LHCb Collaboration, R Aaij et al., Measurement of the time-integrated CP asymmetry in $D^0 \rightarrow K^+K^-$ decays, *Phys Rev Lett* **131**, 091802 (2023).
- [5] Lenz A, Wilkinson G, Mixing and CP violation in the charm system, *Ann Rev Nucl Part Sci* **71**, 59-85 (2021).
- [6] Bause R, Gisbert H, Hiller G, et al., U-spin-CP anomaly in charm, *Phys Rev D* **108**, 035005 (2023).
- [7] Schacht S, A U-spin anomaly in charm CP violation, *J High Energy Phys* **03**, 205 (2023).
- [8] Cheng HY, Chiang CW, Revisiting CP violation in $D \rightarrow PP$ and VP decays, *Phys Rev D* **100**, 093002 (2019).
- [9] Bediaga I, Frederico T, Magalhães PC, Enhanced charm CP asymmetries from final state interactions, *Phys Rev Lett* **131**, 051802 (2023).
- [10] Pich A, Solomonidi E, Vale Silva L, Final-state interactions in the CP asymmetries of charm-meson two-body decays, *Phys Rev D* **108**, 036026 (2023).
- [11] LHCb Collaboration, R Aaij et al., Observation of charge-parity symmetry breaking in baryon decays, arXiv:2503.16954, 2025.
- [12] Lee TD, Yang CN, General partial wave analysis of the decay of a hyperon of spin 1/2, *Phys Rev* **108**, 1645-1647 (1957).
- [13] BESIII Collaboration, M Ablikim et al., First measurement of the decay asymmetry in the pure W-boson-exchange decay $\Lambda_c^+ \rightarrow \Xi^0 K^+$, *Phys Rev Lett* **132**, 031801 (2024).
- [14] Wang HJ, Li PR, Lyu XR, et al., Remarks on strong phase shifts in weak nonleptonic baryon decays, *Sci Bull* **70**, 1183-1185 (2025).
- [15] He XG, Shi YJ, Wang W, Unification of flavor SU(3) analyses of heavy hadron weak decays, *Eur Phys J C* **80**, 359 (2020).
- [16] Yan TM, Cheng HY, Cheung CY, et al., Heavy quark symmetry and chiral dynamics, *Phys Rev D* **46**, 1148-1164 (1992) [erratum: *Phys Rev D* **55**, 5851 (1997)].
- [17] Geng CQ, Liu CW, Tsai TH, Asymmetries of anti-triplet charmed baryon decays, *Phys Lett B* **794**, 19-28 (2019).
- [18] Huang F, Xing ZP, He XG, A global analysis of charmless two-body hadronic decays for anti-triplet charmed baryons, *J High Energy Phys* **03**, 143 (2022) [erratum: *J High Energy Phys* **09**, 087 (2022)].
- [19] Zhong H, Xu F, Wen Q, et al., Weak decays of antitriplet charmed baryons from the perspective of flavor symmetry, *J High Energy Phys* **02**, 235 (2023).
- [20] Xing ZP, He XG, Huang F, et al., Global analysis of measured and unmeasured hadronic two-body weak decays of antitriplet charmed baryons, *Phys Rev D* **108**, 053004 (2023).
- [21] Geng CQ, He XG, Jin XN, et al., Complete determination of $SU(3)_F$ amplitudes and strong phase in $\Lambda_c^+ \rightarrow \Xi^0 K^+$, *Phys Rev D* **109**, L071302 (2024).
- [22] Zhong H, Xu F, Cheng HY, Topological diagrams and hadronic weak decays of charmed baryons, arXiv:2401.15926, 2024.
- [23] Zhong H, Xu F, Cheng HY, Analysis of hadronic weak decays of charmed baryons in the topological diagrammatic approach, *Phys Rev D* **109**, 114027 (2024).
- [24] Buchalla G, Buras AJ, Lautenbacher ME, Weak decays beyond leading logarithms, *Rev Mod Phys* **68**, 1125-1144 (1996).
- [25] Li Hn, Lu CD, Yu FS, Branching ratios and direct CP asymmetries in $D \rightarrow PP$ decays, *Phys Rev D* **86**, 036012 (2012).
- [26] Körner JG, Octet behaviour of single-particle matrix elements $\langle B'|H(W)|B\rangle$ and $\langle M'|H(W)|M\rangle$ using a weak current current quark Lagrangian, *Nucl Phys B* **25**, 282-290 (1971).
- [27] Pati JC, Woo CH, Delta I = 1/2 rule with fermion quarks, *Phys Rev D* **3**, 2920-2922 (1971).
- [28] Groote S, Körner JG, Topological tensor invariants and the current algebra approach: analysis of 196 nonleptonic two-body decays of single and double charm baryons – a review, *Eur Phys J C* **82**, 297 (2022).
- [29] Garrote RA, Cuervo J, Magalhães PC, et al., Dispersive $\pi\pi \rightarrow K\bar{K}$ amplitude and giant CP violation in B to three light-meson decays at LHCb, *Phys Rev Lett* **130**, 201901 (2023).
- [30] Buras AJ, Gerard JM, Ruckl R, 1/N expansion for exclusive and inclusive charm decays, *Nucl Phys B* **268**, 16-48 (1986).
- [31] Bauer M, Stech B, Wirbel M, Exclusive nonleptonic decays of D, D(s), and B mesons, *Z Phys C* **34**, 103 (1987).
- [32] General IJ, Cotanch SR, Goldberger-Treiman constraint criteria for hyperon coupling constants, *Phys Rev C* **69**, 035202 (2004).
- [33] Particle Data Group, S Navas et al., Review of particle physics, *Phys Rev D* **110**, 030001 (2024).
- [34] BESIII Collaboration, M Ablikim et al., Measurements of $K_S^0 - K_L^0$ asymmetries in the decays $\Lambda_c^+ \rightarrow pK_{L,S}^0, pK_{L,S}^0\pi^+\pi^-$, and $pK_{L,S}^0\pi^0$, *J High Energy Phys* **09**, 007 (2024).
- [35] Belle Collaboration, I Adachi et al., Measurements of the branching fractions of $\Xi_c^0 \rightarrow \Xi^0\pi^0$, $\Xi_c^0 \rightarrow \Xi^0\eta$, and $\Xi_c^0 \rightarrow \Xi^0\eta'$ and asymmetry parameter of $\Xi_c^0 \rightarrow \Xi^0\pi^0$, *J High Energy Phys* **10**, 045 (2024).
- [36] LHCb Collaboration, R Aaij et al., Measurement of Λ_b^0, Λ_c^+ , and Λ decay parameters using $\Lambda_b^0 \rightarrow \Lambda_c^+ h^-$ decays, *Phys Rev Lett* **133**, 261804 (2024).

- [37] BESIII Collaboration, M Ablikim et al., Observation of the singly Cabibbo-suppressed decay $\Lambda_c^+ \rightarrow p\pi^0$, Phys Rev D **111**, L051101 (2025).
- [38] BESIII Collaboration, M Ablikim et al., Observation of a rare beta decay of the charmed baryon with a graph neural network, Nat Commun **16**, 681 (2025).
- [39] Belle-II Collaboration, I Adachi et al., Observations of the singly Cabibbo-suppressed decays $\Xi_c^+ \rightarrow pK_S^0$, $\Xi_c^+ \rightarrow \Lambda\pi^+$, and $\Xi_c^+ \rightarrow \Sigma^0\pi^+$ at Belle and Belle II, J High Energy Phys **03**, 061 (2025).
- [40] BESIII Collaboration, M Ablikim et al., Measurements of weak decay asymmetries of $\Lambda_c^+ \rightarrow pK_S^0$, $\Lambda\pi^+$, $\Sigma^+\pi^0$, and $\Sigma^0\pi^+$, Phys Rev D **100**, 072004 (2019).
- [41] Farrell C, Meinel S, $\Xi_c \rightarrow \Xi$ form factors from lattice QCD with domain-wall quarks: a new piece in the puzzle of Ξ_c^0 decay rates, arXiv:2504.07302, 2025.
- [42] He XG, Huang F, Wang W, SU(3) symmetry and its breaking effects in semileptonic heavy baryon decays, Phys Lett B **823**, 136765 (2021).
- [43] Deshpande NG, He XG, CP asymmetry relations between $\bar{B}^0 \rightarrow \pi\pi$ and $\bar{B}^0 \rightarrow \pi K$ rates, Phys Rev Lett **75**, 1703-1706 (1995).
- [44] Wang D, Sum rules for CP asymmetries of charmed baryon decays in the $SU(3)_F$ limit, Eur Phys J C **79**, 429 (2019).
- [45] Cheng HY, Chiang CW, Two-body hadronic charmed meson decays, Phys Rev D **81**, 074021 (2010).
- [46] Schacht S, Soni A, Enhancement of charm CP violation due to nearby resonances, Phys Lett B **825**, 136855 (2022).
- [47] Belle Collaboration, L Li et al., Search for CP violation and measurement of branching fractions and decay asymmetry parameters for $\Lambda_c^+ \rightarrow \Lambda h^+$ and $\Lambda_c^+ \rightarrow \Sigma^0 h^+$ ($h = K, \pi$), Sci Bull **68**, 583-592 (2023).
- [48] LHCb Collaboration, R Aaij et al., Prompt Λ_c^+ production in pPb collisions at $\sqrt{s_{NN}} = 5.02$ TeV, J High Energy Phys **02**, 102 (2019).
- [49] Apollinari G, Béjar Alonso I, Brüning O, et al., High-luminosity large hadron collider (HL-LHC): technical design report V. 0.1, doi:10.23731/CYRM-2017-004.
- [50] Achasov M, Ai XC, Aliberti R, et al., STCF conceptual design report (volume 1): physics & detector, Front Phys (Beijing) **19**, 14701 (2024).
- [51] Cheng HY, Lyu XR, Xing ZZ, Charm physics in the high-luminosity super τ -charm factory, Chin Phys Lett **42**, 010201 (2025).